Journal of Alloys and Compounds 498 (2010) 62–70

Contents lists available at ScienceDirect

Journal of Alloys and Compounds

journal homepage: www.elsevier.com/locate/jallcom

Kinking nonlinear elastic deformation of Ti_3AlC_2, Ti_2AlC, $Ti_3Al(C_{0.5},N_{0.5})_2$ and $Ti_2Al(C_{0.5},N_{0.5})$

A.G. Zhou*, M.W. Barsoum

Department of Materials Science and Engineering, Drexel University, Philadelphia, PA 19104, USA

ARTICLE INFO

Article history:
Received 27 August 2009
Received in revised form 6 March 2010
Accepted 8 March 2010
Available online 15 March 2010

Keywords:
Ceramics
Elasticity
Solid solution
Modeling

ABSTRACT

In this paper four ternary MAX phases, Ti_3AlC_2, Ti_2AlC, $Ti_3Al(C_{0.5},N_{0.5})_2$ and $Ti_2Al(C_{0.5},N_{0.5})$, were fabricated by hot pressing or hot isostatic pressing. The microstructures were characterized and found to be comprised of plate-like grains, 70–130 μm in diameter and 5–10 μm thick. Because all compositions traced fully reversible, reproducible, hysteretic loops during uniaxial cyclic compression tests they were classified as kinking nonlinear elastic (KNE) solids. When the results were analyzed using our recently developed microscale incipient kink band (IKB) model, the various relationships predicted among the three independently measured values – stress, nonlinear strain and dissipated energy – were exceptionally well adhered to. From the results we estimate the critical resolved shear stresses, CRSS, of the basal plane dislocations to range from 24 to 60 MPa. We also show that the relationship between the CRSS and grain size is of a Hall-Petch type. The reversible dislocation density is estimated to be $(1–9) \times 10^{13}$ m^{-2} at stresses that ranged from ≈300 to 650 MPa.

1. Introduction

Kinking nonlinear elastic (KNE) solids – a recently identified class of materials – are so described because they deform nonlinearly, but fully reversibly, i.e. elastically by the formation of dislocation-based kink bands [1–6]. The only requirement for a solid to be KNE is plastic anisotropy, a good measure of which is the c/a ratio in hexagonal crystals. The latter insures that anything but basal slip is energetically unfavorable. KNE solids include the MAX phases (see below) [1,2,5,7,8], graphite [3], hexagonal closed packed metals (Ti, Mg, and Co) [9,10], $LiNbO_3$ [11], ZnO [12], mica [13] among many others.

Cyclic stress–strain curves of KNE solids are characterized by large, closed hysteretic loops. The first KNE solid identified was Ti_3SiC_2 [5], which is the most studied member of the $M_{n+1}AX_n$ phases (or MAX phases). The MAX phases are machinable, layered ternary carbides or nitrides, where M is an early transition metal, A an A group element, X carbon and/or nitrogen, and $n = 1–3$ [14–16]. More recently, we have shown that Ti_2AlC [1] and Cr_2GeC [7] are KNE solids. All MAX phases are believed to be KNE solids because of their high c/a ratios [1,2], which, as noted above, ensures plastic anisotropy.

The KNE behavior of the MAX phases is affected by several factors. Currently, the effects of two microstructure variables, grain size [2,5,17] and porosity [1,8], are reasonably well understood. At comparable stress levels, coarse-grained samples have larger hysteretic loops than their fine-grained counterparts [2,5,17]; porous samples have larger loops than their dense counterparts [1,8]. In our previous work on Ti_2AlC [1] we showed that a 10% porous sample dissipated *more* energy per cycle per unit volume W_d on an *absolute* scale than its fully dense counterpart. This result is probably the strongest evidence to date that our conjecture is valid for the simple reason in that it eliminates any mechanisms, such as dislocation pileups, that scale directly with the volume of the material tested. It is, however, in full agreement with our IKB model in that kinking is a form of plastic instability, or buckling, and thus a less rigid solid is more prone to kinking that a fully dense one. Similar conclusions were reached for porous Ti_3SiC_2 samples, where the enhancements in W_d could be accounted for by a reduction in shear moduli, G [8].

One of the attractive attributes of the MAX phases, and one that should in principle render them technologically potentially quite useful, is the very large combinations of solid solution possibilities. Both the M- and A-atoms can be substituted for each other, with concomitant effects on properties. Of special interest in this work are substitutions on the X-sites; when C is replaced by N, a significant solid solution hardening effect is observed at room temperature [15]. As far as we are aware, Ref. [15] is the only paper in which the effect of solid solutions on the X-sites on the mechanical properties of MAX phases has been explored in any detail. Others have focused on solid solutions on the A- [18,19] or M-sites [20–22].

---

* Corresponding author. Present address: School of Materials Science and Engineering, Henan Polytechnic University, 2001, Century Avenue, Jiaozuo, Henan 454100, China. Tel.: +86 391 3986936; fax: +86 391 3986908.
E-mail address: zhouag@hpu.edu.cn (A.G. Zhou).

0925-8388/$ – see front matter © 2010 Elsevier B.V. All rights reserved.
doi:10.1016/j.jallcom.2010.03.099

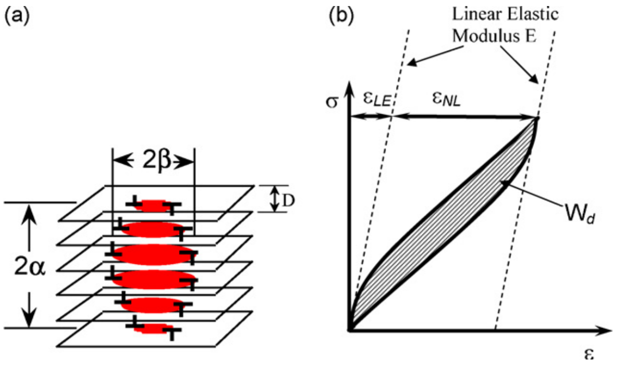

Fig. 1. (a) Schematic of a thin elliptical IKB with length of 2α and width, or diameter, 2β. (b) Typical stress–strain curve for a KNE solid. The various parameters needed to describe the curve are labeled. The energy dissipated per cycle per unit volume, W_d, is the hatched area enclosed by the loops.

Substituting N for C in Ti_2AlC and Ti_3AlC_2 [23] results in a decrease in unit cell parameters and a concomitant increase in phonon conductivity and shear moduli [23,24]. Somewhat surprisingly, the substitution of C by N resulted in a decrease in bulk moduli [23,24]. Replacing all the C by N also results in – depending on the quality of the samples – either an increase or a decrease in phonon conductivity [23]. These anomalous results – most importantly the reduction in elastic moduli with a reduction in unit cell parameters and presumably stronger bonds – have been explained by invoking that the presence of vacancies on the N and/or Al sites as the C is substituted by N [23].

In addition to our work, there have been a few papers in the literature in which fully reversible stress–strain loops have been observed in different, diverse materials [25–31] and in the MAX phases [32–35]. In the case of Mg, most authors ascribe this behavior to reversible twinning [28–30]. Orlovskaya et al. [25] and Hao et al. [26,27] concede they have no good explanations, and suggest that KNE mechanism is a possibility for the deformation of $La_{0.6}Sr_{0.4}FeO_3$ perovskite and titanium alloys, respectively. Most recently, the kink band model was considered to explain the deformation of some clays [36] and ice [37]. None of these papers, however, tested the KNE idea; it was only briefly alluded to.

The purpose of this paper is to examine the effects of X-site substitutions and unit cell structures on the kinking nonlinear response of Ti_3AlC_2 and Ti_2AlC and their solid solutions, $Ti_2Al(C_{0.5}N_{0.5})$ and $Ti_3Al(C_{0.5}N_{0.5})_2$—henceforth referred to as Ti_3AlCN. The only difference between Ti_3AlC_2 and Ti_2AlC is the number of TiC_x layers separating the Al layers: in Ti_3AlC_2 there are two, in Ti_2AlC, one [14]. The solid solutions, $Ti_2Al(C_{0.5}N_{0.5})$ and Ti_3AlCN, on the other hand, have identical unit cells as their corresponding end members, except that half of the C atoms are replaced by N atoms. Before describing the experimental details it is important to briefly review our KNE model, which has been described in detail in previous work [1,2,9,10].

2. KNE model

Frank and Stroh (F&S), considered an elliptic kink band, KB, with length, 2α, and width, 2β, such that $\alpha \gg \beta$ (Fig. 1a) and showed that the remote critical axial stress, σ_t, at the polycrystal level, needed to render such a subcritical KB unstable is given by [2,38]:

$$\tau > \tau_c \approx \frac{\sigma_t}{M} \approx \sqrt{\frac{4G^2 b \gamma_c}{2\alpha\pi^2} \ln\left(\frac{b}{\gamma_c w}\right)} \tag{1}$$

where τ_c, is the local critical shear stress, at the single grain scale. M is the Taylor factor relating σ_t, to τ_c; G is the shear modulus and b is the Burgers vector; w is related to the dislocation core width [38]. In our MAX phase work to date, we equated the grain dimension along the [0 0 0 1] direction – i.e. normal to the direction of easy slip – with 2α [2,8]. If 2α is known, then w can be estimated from Eq. (1) making use of the experimentally determinable σ_t (see below). γ_c is critical kinking angle calculated assuming [9,38,39]:

$$\gamma_c = \frac{b}{D} \approx \frac{3\sqrt{3}(1-\nu)\tau_{\mathrm{loc}}}{2G} \approx \frac{3\sqrt{3}(1-\nu)}{8\pi e}\left(\frac{b}{w}\right) \tag{2}$$

where ν is Poisson ratio and τ_{loc} is the local shear stress needed to nucleate a dislocation pair; D is the distance between dislocation loops along 2α (Fig. 1a). If one assumes, $\tau_{\mathrm{loc}} \approx G/30$, then γ_c is of the order of 3°. Note that assuming $G/30$ implicitly assumes $w = b$ [9]. If as assumed here, $w = 5b$, then γ_c is of the order of 0.06 rad or 1.7°.

An IKB consists of multiple parallel dislocation loops (Fig. 1a). As a first approximation we assume each loop is comprised of two edge and two screw dislocation segments with lengths, $2\beta_x$ and $2\beta_y$, respectively. The latter are related to the applied stress, σ and 2α, assuming [10,38]:

$$2\beta_x \approx \frac{2\alpha(1-\nu)}{G\gamma_c}\frac{\sigma}{M} \quad \text{and} \quad 2\beta_y \approx \frac{2\alpha}{G\gamma_c}\frac{\sigma}{M} \tag{3}$$

The formation of an IKB can be divided into two stages: nucleation and growth [9]. Since the former is not well understood, our model only considers IKB growth from $2\beta_{xc}$ and $2\beta_{yc}$ to $2\beta_x$ and $2\beta_y$, respectively. The dislocation segment lengths of an IKB nucleus, β_{xc} and $2\beta_{yc}$, are presumed to pre-exist, or are nucleated during prestraining. The values of $2\beta_{xc}$ and $2\beta_{yc}$ are estimated from Eq. (3), assuming $\sigma = \sigma_t$; the latter is experimentally obtained (see below).

It follows that for $\sigma > \sigma_t$, the IKB nuclei grow and the IKB-induced axial strain resulting from their growth is assumed to be given by [10]:

$$\begin{aligned}\varepsilon_{\mathrm{IKB}} &= \frac{\Delta V N_k \gamma_c}{k_1} = \frac{N_k \gamma_c 4\pi\alpha(\beta_x\beta_y - \beta_{c,x}\beta_{c,y})}{3k_1} \\ &= \frac{4\pi(1-\nu)N_k\alpha^3}{3k_1 G^2 \gamma_c M^2}(\sigma^2 - \sigma_t^2) = m_1(\sigma^2 - \sigma_t^2)\end{aligned} \tag{4}$$

where m_1 is the coefficient before the term in parentheses in the fourth term; N_k is the number of IKBs per unit volume; ΔV is the volume change due to the growth of one IKB as the stress increases from σ_t to σ. It follows that the volume fraction, v_f, of the material that is kinked is given by $V \times N_k$. The factor k_1 relates the volumetric strain due to the IKBs to the axial strain along the loading direction. The value of k_1 depends on the texture of samples and ranges from 1 to 2. If samples are without texture, k_1 can be assumed to be 2. For example, Reed-Hill et al. [40] assumed $k_1 = 2$ for their work on Zr. Herein $k_1 = 2$ was also assumed.

The energy dissipated per unit volume per cycle, W_d (shaded area in Fig. 1b) resulting from the growth of the IKBs from β_{ic} to β_i is given by [10]:

$$\begin{aligned}W_d &= \frac{4\Omega\pi N_k \alpha}{D}(\beta_x\beta_y - \beta_{xc}\beta_{yc}) \\ &= \frac{4\pi(1-\nu)N_k\alpha^3}{G^2\gamma_c M^2}\frac{\Omega}{b}(\sigma^2 - \sigma_t^2) = m_2(\sigma^2 - \sigma_t^2)\end{aligned} \tag{5}$$

Ω is the energy dissipated by a dislocation line sweeping a unit area. Thus, Ω/b should be proportional, if not equal, to the critical resolved shear stress, CRSS, of an IKB dislocation loop. Herein and in our previous work, we show that to be the case [9,10].

Combining Eqs. (4) and (5) yields:

$$W_d = 3k_1\frac{\Omega}{b}\varepsilon_{\mathrm{IKB}} = \frac{m_2}{m_1}\varepsilon_{\mathrm{IKB}} \tag{6}$$

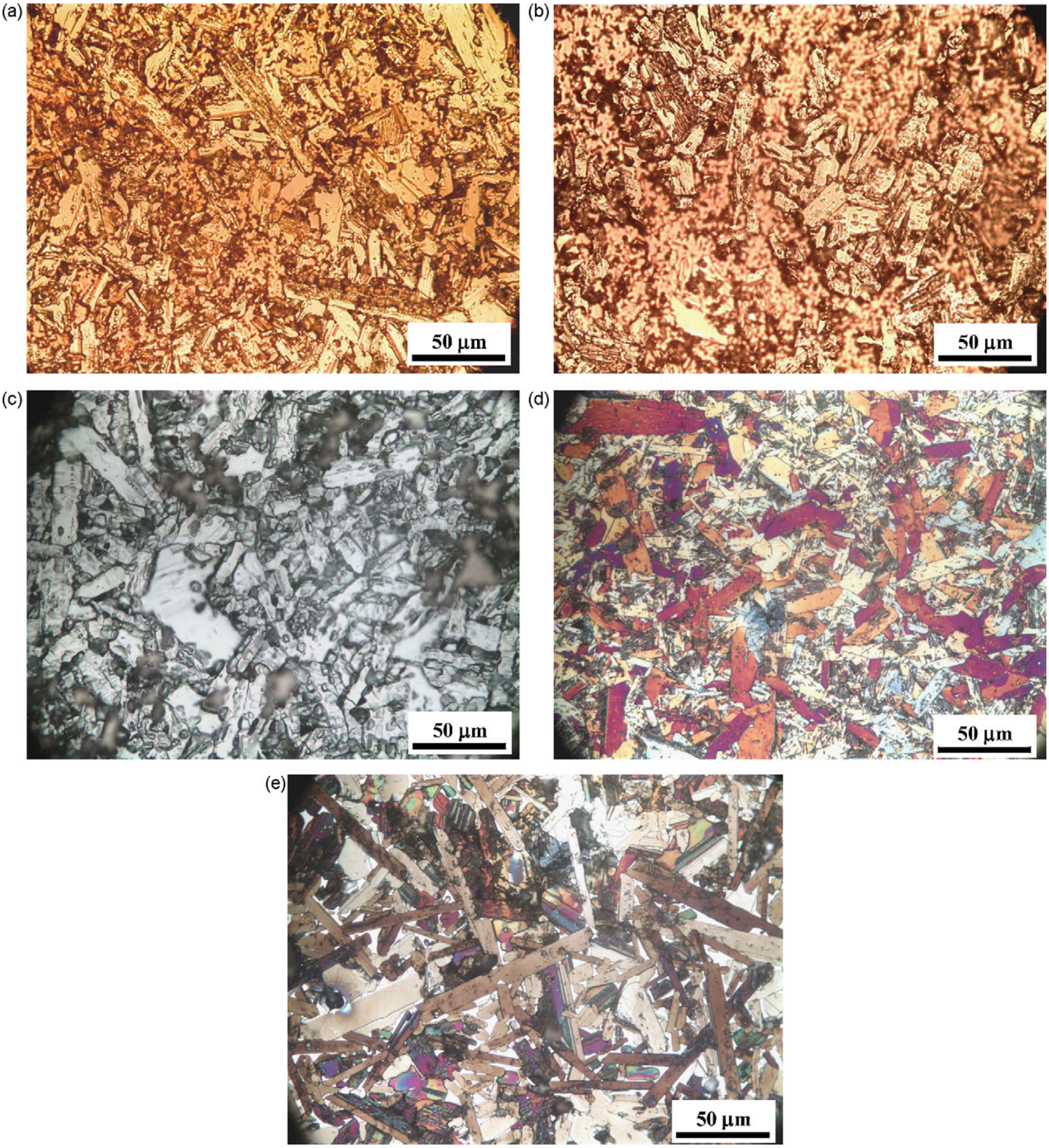

Fig. 2. Optical micrographs of (a) Ti_3AlCN before annealing, (b) $Ti_2Al(CN)$ before annealing, (c) Ti_3AlCN after annealing, (d) Ti_3AlC_2, and (e) Ti_2AlC.

Assuming the IKBs are cylinders with radii β_{av}, then the *reversible* dislocation density, ρ_{rev}, due to the IKBs is given by:

$$\rho_{rev} = \frac{2\pi N_k 2\alpha\beta_{av}}{D} = \frac{4\pi N_k \alpha\beta_{av}\gamma_c}{b} \qquad (7)$$

Experimentally (see below) one can determine σ_t and $3k_1(\Omega/b)$. The estimation of Ω/b only requires knowledge of k_1 in Eq. (6).

To recap: Once nested loops (see below) are obtained and the various relationships, viz. ε_{IKB} vs. σ^2, W_d vs. σ^2, and W_d vs. ε_{NL}, are plotted, Eq. (6) is used to estimate Ω/b, assuming $k_1 = 2$. Experimentally, m_1 and m_2 can be determined from the slopes of ε_{IKB} vs. σ^2 and W_d vs. σ^2 plots, respectively. It follows that if our assumptions are correct, and more importantly, if the micromechanism causing the dependence of ε_{NL} on σ (i.e. Eq. (4)) is the *same* as the one responsible for W_d (Eq. (5)), then the *ratio* m_2/m_1 should equal $3k_1(\Omega/b)$. In other words, if both expressions give the same values for Ω/b that would be strong evidence that our assumptions are correct and more important that the same micromechanism that results in the parabolic dependence of σ on ε_{NL} is also responsible for W_d.

3. Experimental details

The Ti_3AlC_2 sample was made from stoichiometric mixtures of Ti powder (-325 mesh, 99.5%,), Al powder (-325 mesh, 99.5%), and graphite powders (-300 mesh, 99%) all from Alfa Aesar, Ward Hill, MA. After 4 h mixing by ball milling, the powders were annealed at 625 °C for 3 h in a vacuum hot press followed by sintering at 1400 °C for 1 h with a load that corresponded to a pressure of ~45 MPa.

The Ti_2AlC samples were prepared by cold isostatic pressing Ti_2AlC powders with an average particle size, $d_{50} = 8\ \mu m$ (Kanthal, AB, Sweden), followed by pressureless sintering at 1500 °C for 1 h in flowing Ar [1].

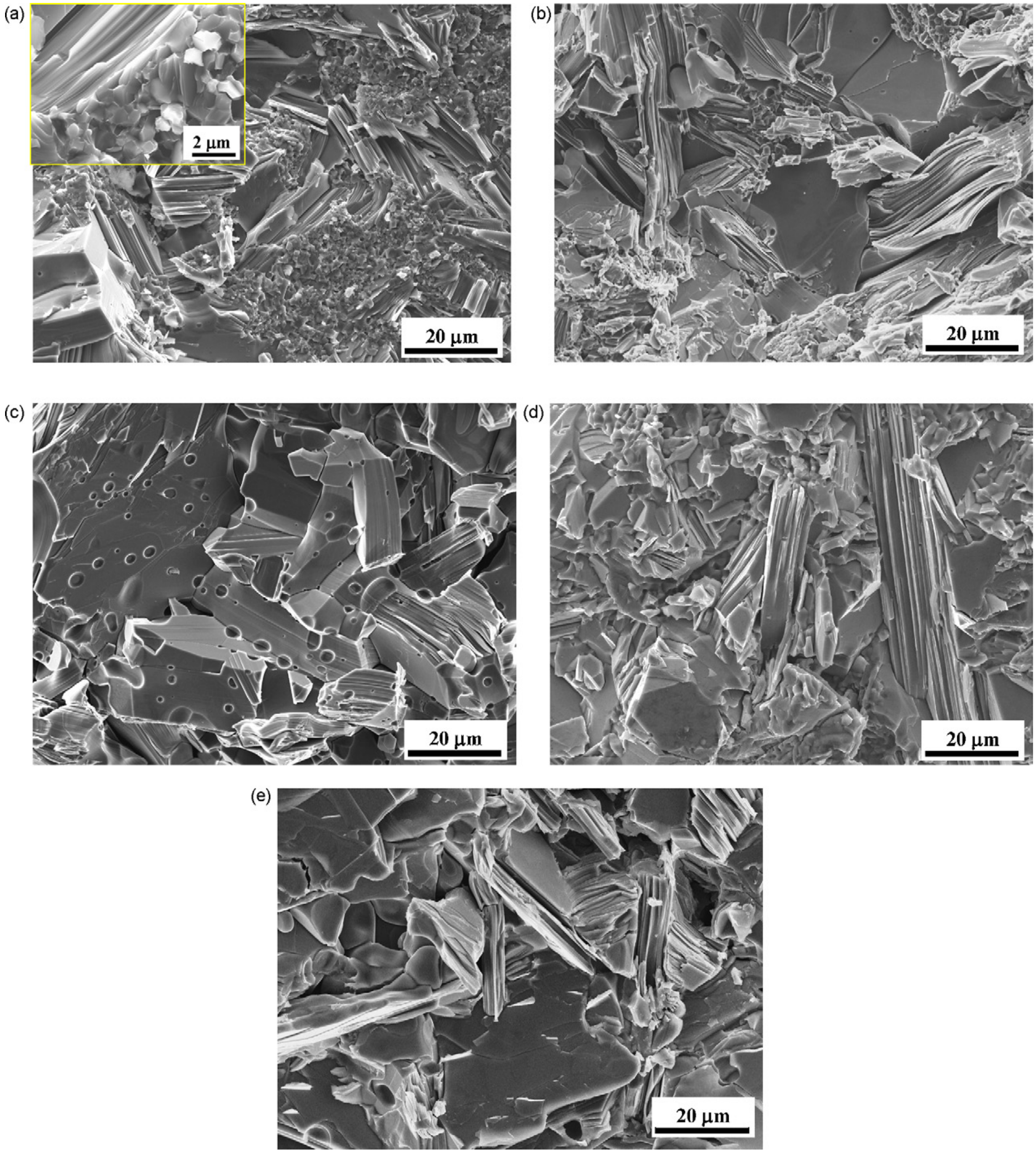

Fig. 3. SEM micrographs of (a) Ti_3AlCN before annealing, (b) Ti_3AlCN after annealing, (c) $Ti_2Al(C_{0.5}N_{0.5})$ after annealing, (d) Ti_3AlC_2, and (e) Ti_2AlC.

The Ti_3AlCN and $Ti_2AlC_{0.5}N_{0.5}$ samples were made from stoichiometric mixtures of Ti, Al, AlN (-200 mesh, 99.0% Cerac, Milwaukee, WI) and graphite powders after overnight ball milling and cold pressing to ≈600 MPa. The green bodies were presintered in a vacuum furnace at 525 °C for 2 h, then at 625 °C for 10 h. The presintered pellets were then reacted and densified in a hot isostatic press (HIP) at temperature of 1400 °C under a pressure of 100 MPa for 10 h [41]. To grow the solid solution samples' grains, they were annealed at 1400 °C for 48 h in flowing Ar gas.

X-ray diffraction, XRD (Siemens D-500) was used to identify the phases present. A scanning electron microscope, SEM (FEI/Phillips XL30, Hillsboro, OR) was used to examine the fractured surfaces and an optical microscope, OM (Olympus PMG-3, Tokyo, Japan) to examine polished and etched surfaces. The etchant was $HF:HNO_3:H_2O = 1:1:1$ [16].

The details of the compression experiments can be found elsewhere [1,2,42]. Briefly, 9.7 mm diameter, 312 mm long cylinders were electro-discharge machined and cyclically compressed to different stress levels using a hydraulic testing machine (MTS 810, Minneapolis, MN), supplied with a controller (Microconsoler 458.20, MTS). The strain was measured using an extensometer (MTS 632.59C-01), with a gauge length of 25 mm, directly attached to the samples. In most KNE solids, a small plastic deformation is usually recorded during the first cycle; all subsequent cycles to the same stress are closed and fully reproducible. The analysis was carried out on the latter, and for the most part, are the ones shown here.

4. Results

4.1. Microstructural characterization

The purity and lattice parameters of as-synthesized samples can be calculated from XRD spectra (not shown) and were reported in previous papers [15,41,43]. All samples were predominantly single phase with impurities of ~5 vol.% TiC and ~3 vol.% Al_2O_3. The *a*- and *c*-lattice parameters of Ti_3AlCN were 3.0404 Å and 18.414 Å, respectively [41]; those of Ti_3AlC_2 were $a = 3.0654$ Å and $c = 18.487$ Å [43]. For $Ti_2AlC_{0.5}N_{0.5}$, $a = 3.021$ Å, $c = 13.610$ Å and for Ti_2AlC, $a = 3.051$ Å and $c = 13.637$ Å [15]. Clearly, and in full agreement with previous work, the solid solutions had smaller lattice parameters than their corresponding C-containing end members.

OM and SEM micrographs of some of the samples fabricated herein are shown in Figs. 2 and 3, respectively. OM micrographs of the as-fabricated Ti_3AlCN and $Ti_2Al(C_{0.5},N_{0.5})$ samples, shown respectively in Fig. 2a and b, showed they comprised two grain sizes; large plate-like grains, and smaller equiaxed grains. The stark difference in the grain sizes is more clearly shown in the SEM micrograph of a Ti_3AlCN fractured surfaces (Fig. 3a). The $Ti_2Al(C_{0.5},N_{0.5})$ samples looked almost identical to those of Ti_3AlCN and are not shown. This duplex microstructure is similar to that observed in Ti_3SiC_2 [44], and occurs when the holding time at the processing temperatures is insufficient for the full coarsening of the microstructure to occur. Because grain growth is faster along the *a*-direction than the *c*-direction, the latter grow as hexagonal plates, with their large dimension along the *a*-direction [44].

To rid the solid solutions of the fine-grains, they were annealed at 1400 °C for 48 h. From the resulting microstructure of Ti_3AlCN (Figs. 2c and 3b) it is clear that the sample remained fully dense and that most of the small grains disappeared, with little growth in the size of the coarse grains. In the case of $Ti_2Al(C_{0.5}N_{0.5})$, in addition to the disappearance of many of the smaller grains, a multitude of pores appeared (Fig. 3c). The reasons for the formation of these pores are not understood at this time, but may be due to an incipient dissociation and the formation of nitrogen gas. The formation of nitrogen gas and possible loss of Al at high temperatures can also convert $Ti_2Al(C_{0.5}N_{0.5})$ to TiC. In a previous paper [8], the influence of porosity and TiC impurities on the nonlinear deformation of Ti_3SiC_2 was discussed in detail. Herein, the discussion is focused on the effect of grain size.

Figs. 2d, 2e, 3d and 3e show the microstructures of the Ti_3AlC_2 and Ti_2AlC samples, respectively. When these micrographs are compared to those of annealed Ti_3AlCN (Figs. 2c and 3b), it is reasonable to assume that all samples used in this work had comparable plate-like grains 70–130 μm in diameter, that were 5–10 μm thick. For calculation purposes, however, the values of 2α for all microstructures were calculated from their respective σ_t values using Eq. (1) (see below).

4.2. Cyclic compression results

Typical stress–strain curves – progressively shifted to the right for clarity – for the $Ti_2Al(C_{0.5}N_{0.5})$ sample are shown in Fig. 4a. At stress levels below 400 MPa, the response of the virgin sample (curve A) was linear elastic with a Young's modulus of 291 GPa. At 620 MPa, fully reversible, hysteretic loops (curve B) are present. At 720 MPa, the hysteretic loops are larger (curve C) but are not fully reversible; a very small plastic deformation is recorded at this stress. It is important to emphasize that the extent of the plastic deformation is quite small. When the sample was unloaded, and reloaded to 620 MPa (curve D) the loops were slightly larger than upon loading the first time, i.e. curve B. When the sample was reloaded to a stress of 400 MPa, a small loop is observed where *none* existed for the virgin sample (compare internal loop in D, with A).

Compared with this fully dense sample, the annealed $Ti_2Al(C_{0.5}N_{0.5})$ sample, curve E, showed a much lower effective modulus and large loops even at 250 MPa. The values of the Young's moduli determined from the slopes of the dashed lines that are tangent to the loops during initial unloading (see Fig. 4) were in good agreement with values reported in the literature on similar samples measured by ultrasound [23] and shown in the second column in Table 1.

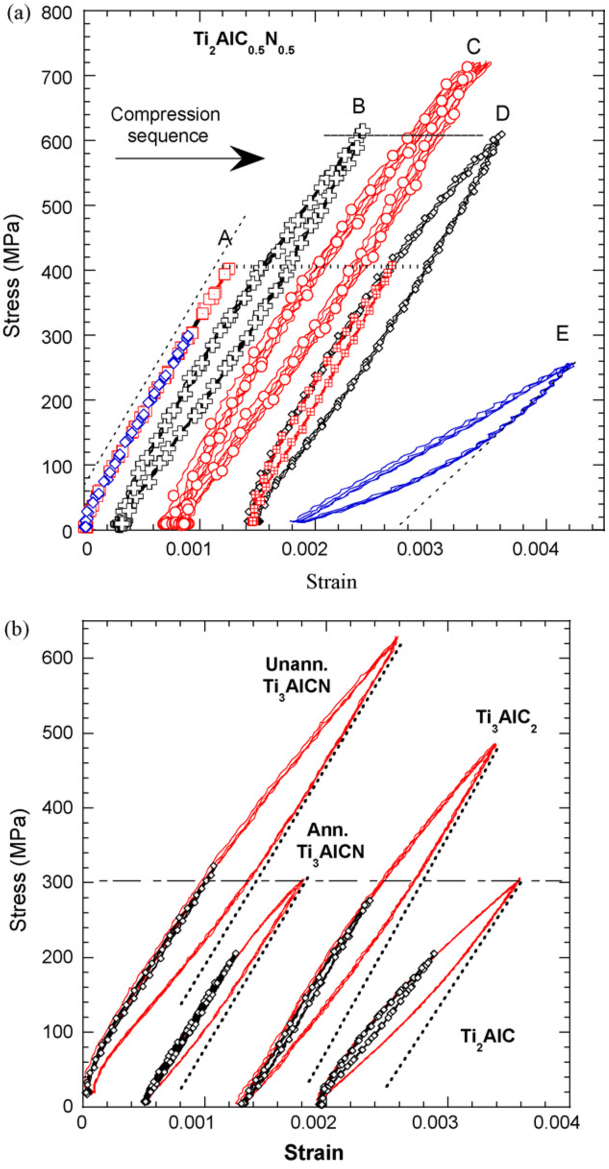

Fig. 4. (a) Stress–strain curves of $Ti_2Al(C_{0.5}N_{0.5})$ sample—progressively shifted to the right for clarity. Curves A–D are for an un-annealed sample by the testing sequence from A to D. Curve E is for the annealed sample. (b) Stress–strain curves of Ti_3AlCN, Ti_3AlC_2 and Ti_2AlC.

Fully reversible hysteretic stress–strain loops were also recorded for Ti_3AlCN, Ti_3AlC_2 and Ti_2AlC (Fig. 4b). At ∼300 MPa – horizontal line in Fig. 4b – the response of un-annealed Ti_3AlCN is linear elastic. Annealing reduces the threshold stress and fully reversible loops are observed at stresses <300 MPa (Fig. 4b). Note the Young's moduli for Ti_3AlCN did not change upon annealing; those for $Ti_2Al(C_{0.5}N_{0.5})$ did, presumably as a result of the formation of porosity.

Both the Ti_3AlC_2 and Ti_2AlC samples exhibited similar loops (Fig. 4b). Compared with Ti_3AlC_2, Ti_2AlC has a lower Young's modulus (Table 1), but larger hysteretic loops at ∼300 MPa.

4.3. Application of KNE model

Based on the preceding discussion, the mechanical hysteresis of a KNE solid can be characterized by three parameters, σ, ε_{NL} and W_d—listed in Table 2. According to Eqs. (4)–(6), plots of ε_{NL} vs. σ^2,

Table 1
List of physical constants, E, G, ν, used in calculations. The values of 2α are calculated from the σ_t listed in column 6, obtained experimentally. The last column lists the values of σ_t estimated from the point at which the stress–strain curves deviate from linearity. The values listed below for Ti_2AlC are different than those reported previously [1], because the assumed value of M (see below) was changed from 2 to 3. Also included are results for Ti_3SiC_2 and Cr_2GeC [7]. With the exception of Cr_2GeC, w and b were assumed to be $5b$ and 3.07 Å, respectively. b for Cr_2GeC is 2.95 Å. Unless otherwise noted, elastic properties were obtained from Ref. [23].

	E (GPa)	G (GPa)	ν	2α (μm)	σ_t [a] (MPa)	σ_t [b] (MPa)
Ti_3AlC_2	298	124	0.2	10	244	205
Un-ann. Ti_3AlCN	330	137	0.2	7	317	286
Ann. Ti_3AlCN			0.2	22	180	160
$Ti_2Al(C_{0.5},N_{0.5})$	290	123	0.2	4.1	376	295
Ti_2AlC	277	118	0.2	18	170	98
Ti_3SiC_2	325	144	0.2	42	138	–
Cr_2GeC	245 [7]	80 [7]	0.3	26.7	90	–

[a] From W_d vs. σ^2 plots (Fig. 5b).
[b] From stress–strain curves (Fig. 4).

Table 2
List of stress σ, nonlinear strain, ε_{NL}, and dissipated energy W_d for Ti_3AlC_2, Ti_2AlC, $Ti_2Al(C_{0.5}N_{0.5})$ and Ti_3AlCN samples tested herein.

	σ (MPa)	ε_{NL}	W_d (MJ/m^3)	m_1 (MPa)$^{-2}$	m_2 (MPa)$^{-1}$	m_2/m_1 (MPa)
Ti_3AlC_2	280	0.00017	0.011	2.2×10^{-9}	4.9×10^{-7}	217
	349	0.00025	0.029			
	417	0.00038	0.054			
	486	0.00051	0.087			
Ti_2AlC	205	0.00023	0.015	6.9×10^{-9}	9.7×10^{-7}	141
	237	0.00032	0.027			
	271	0.00042	0.042			
	306	0.00059	0.061			
	336	0.00071	0.085			
$Ti_2Al(C_{0.5}N_{0.5})$	462	0.00018	0.048	1.7×10^{-9}	6.2×10^{-7}	370
	511	0.00024	0.073			
	561	0.00034	0.102			
	610	0.00044	0.146			
Ti_3AlCN un-annealed	321	0.00010	0.009	1.4×10^{-9}	4.4×10^{-7}	312
	426	0.00017	0.028			
	526	0.00033	0.074			
	629	0.00050	0.136			
Ti_3AlCN annealed	156	0.00008	0.001	2.8×10^{-9}	5.0×10^{-7}	182
	206	0.00009	0.006			
	255	0.00014	0.015			
	305	0.00023	0.031			

W_d vs. σ^2 and W_d vs. ε_{NL} should all yield straight lines, as observed in Fig. 5. The lowest correlation coefficient, R^2, value is >0.98.

Table 1 lists the physical constants assumed, as well as the values of 2α calculated from σ_t – listed in column 6 – using Eq. (1) and γ_c from Eq. (2). The threshold stress, σ_t, was obtained by two different methods. The first is from the W_d vs. σ^2 plots (Fig. 5b). According to Eq. (5), the x-axis intercept in Fig. 5b is σ_t, referred to as σ_t^* (column 6 in Table 1). The second method is from the point at which the stress–strain curves deviate from linearity, henceforth referred to as $\sigma_t^\ddagger$ (column 7 in Table 1). The one used to calculate 2α is σ_t^*.

Lastly, based on the results shown in Fig. 5, Table 1 and Eqs. (3)–(7), the values of Ω/b, N_k, $2\beta_{av,c}$ and $2\beta_{av}$, ρ_{rev} were calculated and are listed in Table 3. In all the calculations, M and k_1 were assumed to be 3 and 2, respectively. For why $M = 3$ refer to [45].

5. Discussion

Clearly all solids tested herein are KNE solids, with the unit cell structure, solid solution, grain-size distributions and preload histories all influencing σ_t and the shapes and areas of the hysteresis loops.

In previous studies on the MAX phases, it was assumed that σ_t was independent of deformation history [1,2,5]. It is now apparent this is not always the case. For example, during the nanoindenta-

Table 3
Calculated values of Ω/b, N_k and $2\beta_{av,c}$, the latter calculated at the σ_t^* values listed in Table 2 The $2\beta_{av}$ and ρ_{rev} values at the σ values listed in column 9 are listed in columns 7 and 8, respectively. The last 2 columns compare the nonlinear strains calculated from Eq. (4) using the values reported in this table and the measured σ values listed in column 9 and those experimentally measured (last column). For all cases, $M = 3$, $w = 5b$, $k_1 = 2$ and the 2α values listed in Table 2 were assumed.

	$\Omega//b$ (MPa) Eq. (5)	Ω/b (MPa) Eq. (6)	N_k (m^{-3})	$(1/N_k)^{1/3}$ (μm)	$2\beta_{av,c}$ (μm)	$2\beta_{av}$ (μm)	ρ_{rev} (m^{-2})	σ (MPa)	$\varepsilon_{NL\ Cal.}$	$\varepsilon_{NL\ Meas.}$
Ti_3AlC_2	36	36	1.8×10^{16}	4	0.48	0.95	4.3×10^{13}	486	0.00052	0.00051
Un-ann. Ti_3AlCN	53	53	3.8×10^{16}	3	0.4	0.8	5.4×10^{13}	629	0.00056	0.00050
Ann. Ti_3AlCN	30	31	2.5×10^{15}	7.4	0.7	1.2	1.7×10^{13}	305	0.00026	0.00023
$Ti_2Al(C_{0.5},N_{0.5})$	62	62	2.0×10^{17}	1.7	0.3	0.5	1.0×10^{14}	610	0.00064	0.00044
Ti_2AlC	24	24	8.0×10^{15}	5	0.65	1.3	4.8×10^{13}	336	0.00078	0.00071
Ti_3SiC_2	30	30	4.9×10^{14}	13	1.0	2.6	1.3×10^{13}	366	0.00044	0.00038
Cr_2GeC [7]	22	22	3.6×10^{15}	6.6	0.8	4.6	1.0×10^{14}	525	0.0059	0.0060

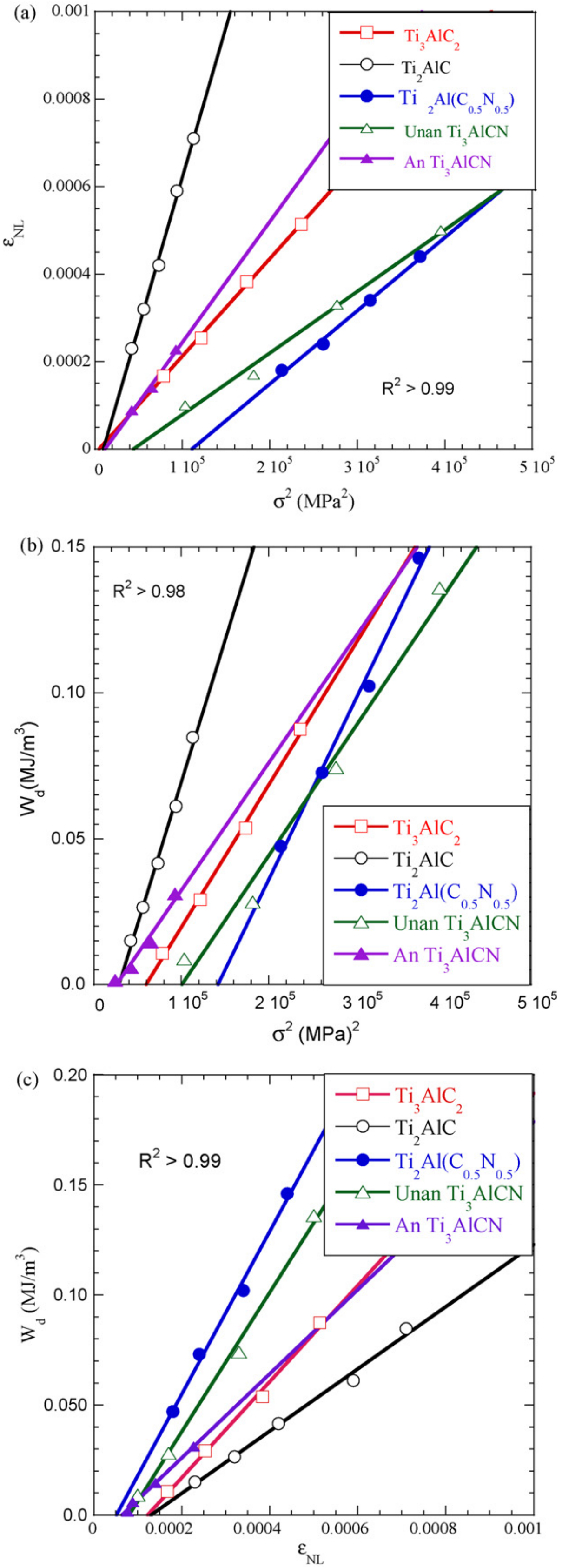

Fig. 5. (a) Plot of ε_{NL} vs. σ^2 for the samples tested in this paper. (b) Plot of W_d vs. σ^2. (c) Plot of W_d vs. ε_{NL}.

tion of single crystals of ZnO, GaN, $LiNbO_3$, and sapphire pop-ins resulted in the formation of multiple domains that rotate basal planes into directions of shear, in some cases greatly enhancing IKB activity. The same is true of polycrystalline Mg [10,28] Zr [40] and Co; a small plastic deformation is sometimes needed to initiate IKB activity. The results shown in Fig. 4a, confirm this notion: it was only after the sample was loaded to 700 MPa that loops were seen at 400 MPa. The mechanism by which this occurs is unclear, but the formation of dislocation pileups and/or mobile dislocation walls, MDWs, maybe implicated. Microcracking and grain boundary sliding cannot be ruled out at this time. This comment notwithstanding, it is hereby acknowledged that IKB nucleation is not understood. However, better understanding is important because if understood, it may be possible to endow otherwise brittle solids with some limited ductility.

The fact that at the same stress level the porous $Ti_2Al(C_{0.5},N_{0.5})$ sample can dissipate significantly more energy than a fully dense one (compare curve E with other curves in Fig. 4a), is not a surprise and is in line with previous results [1,8]. It is however, an important clue as to what is happening, and strongly confirms that what is observed is due to IKBs because, as we noted previously [1], it essentially eliminates any deformation mechanism that scales with the volume of the material.

The effect of n, viz. the number of $Ti_{n+1}X_n$ layers, on kinking is best seen in Fig. 4b. Ti_2AlC is a softer material than Ti_3AlC_2 and consequently, at the same stress level, has larger hysteretic loops. The extra TiC layer also increases Ω/b from ≈24 to 30–36 MPa (Table 3).

When the two un-annealed solid solution compositions are loaded it is apparent that the σ_ts increase significantly. The simplest explanation is that the small equiaxed grains (Figs. 2a, 2b and 3a) prevent or constrain the larger grains from kinking. The small grains, whose influence is essentially the opposite of pores, result in a decrease in the average 2α, and hence an increase in σ_t. The values of 2α calculated for the various microstructures are listed in Table 1, and are comparable to the widths of the grains shown in Figs. 2 and 3. Note that the values of 2α calculated from the model are an "equivalent" average grain size. These values will always be greater than the largest grains. It is also for this reason that the values of σ_t calculated from W_d vs. σ^2 plots are always greater than those directly obtained from where the stress–strain curves deviate from linearity. The latter depend on the largest and most favorably oriented grains to kinking rather than the "average".

The changes in Ω/b for these two compositions is less clear, however. Based on the results shown in Fig. 5b and the values of Ω/b listed in Table 3, it would be reasonable to conclude that what is observed is an increase in the CRSS due to solid solution strengthening. And while tempting and, possibly, at least partially, correct the results for the annealed Ti_3AlCN sample suggest otherwise. Since it is not clear why annealing would result in an almost 2-fold decrease in Ω/b this explanation is suspect.

The second, and more likely explanation, is that the effect observed is essentially a Hall-Petch effect in which Ω/b, a measure of "yield", is a function of grain size. This explanation is bolstered by the results shown in Fig. 6, where Ω/b is plotted as a function of $1/\sqrt{2\alpha}$. A least squares analysis of the data result in an $R^2 > 0.93$. Why the intercept of the best-fit line intersects the x-axis instead of the y-axis as it should is not clear at this time and leaves the door open to other interpretations. Note we have previously shown that in Ti_3SiC_2, Ω/b is also a function of grain size [2].

Regardless of the values obtained for the various microstructures, the fact that the values of Ω/b calculated by Eqs. (5) and (6), are almost identical is strong evidence that the micromechanism causing the strain nonlinearity is the same as that resulting in W_d. Hence, for example, microcracking as a possible mechanism for W_d can be safely excluded. Lastly, and with the exceptions of

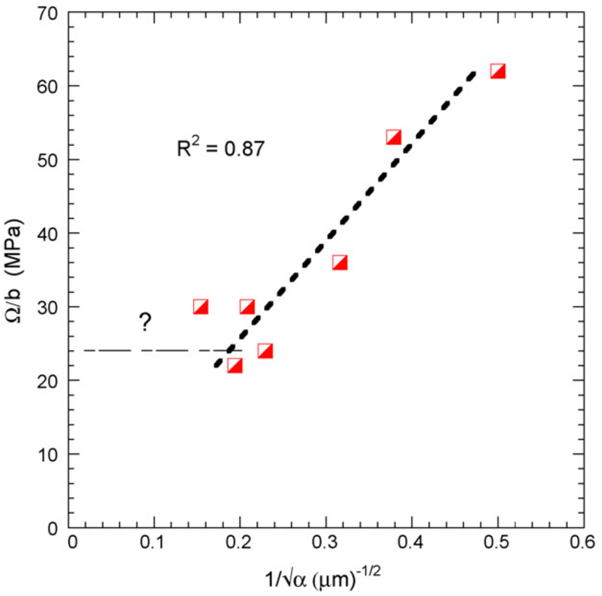

Fig. 6. Plot of Ω/b vs. $1/\sqrt{2\alpha}$.

the two un-annealed solid solution compositions, all the Ω/b values are reasonable and comparable to the only reported value of a CRSS in a MAX phase measured on quasi-single crystals, viz. 36 MPa for Ti_3SiC_2 [46].

At $\approx(1–9)\times 10^{13}\ m^{-2}$, the values of ρ_{rev} are reasonable given the stresses applied. Recall that ρ_{rev} is not the dislocation density in the sample when the load is removed, but rather that which is due solely to the IKBs, given by Eq. (7). What is truly remarkable is that the values of ρ_{rev} vary by less than an order of magnitude despite the fact that the maximum applied stresses and G vary over a factor of 2, and N_k values vary by more than two orders of magnitude (Table 3). This observation suggests that an equilibrium ρ_{rev} exists to which all systems migrate. In solids with high G values and small grains, many small IKBs form; in solids with low G values and coarse grains, fewer, but larger, IKBs form.

As another check on the validity of our method, columns 10 and 11 in Table 3 compare, respectively, the calculated and measured values of ε_{NL}, where the former is calculated from Eq. (4). The agreement between the two sets of results is quite good considering the many simplifying assumptions made.

Lastly the choice of the value of $w = 5b$, needs to be addressed. The minimum value of w is b. This value is impossible herein because it results in 2α values that are unreasonable. For example, assuming $w = b$ for Ti_2AlC, implies – using Eq. (1) and $M = 3$ – a 2α of the order of 100 μm, which is clearly not the case (see Fig. 3e). Recall 2α is the thickness of the grains. Assuming $w = 5b$, implies the width of the *average* grain in Fig. 3e to be 18 μm, which is possible. On the other extreme, assuming $w = 20b$, for $Ti_2Al(C_{0.5}N_{0.5})$ yields 2α values $\approx$1.8 μm, which is again not consistent with the micrograph shown in Fig. 3c. Another more serious problem is that such small 2α values result in N_ks that are so large – $1\times 10^{18}\ m^{-3}$ – as to be difficult to rationalize and would render $V \times N_k$ – or $v_f > 1$. Also the distance between IKBs – estimated to be $(1/N_k)^{1/3}$ – should be of the order of a few microns at least since it is difficult to imagine a much higher density. The values of $(1/N_k)^{1/3}$ calculated here and listed in column 6 of Table 3 fall in the narrow and reasonable range of 1.3–5 μm.

Based on these considerations, we chose a value of $5b$, which is the same value we assumed for the Mg [10] and Co [9]. Note that the choice of w only affects the values of γ_c, 2α and N_k. If future research results in more accurate values of w, then these values would need to be modified accordingly. More importantly, the choice of w does not affect the values of Ω/b.

Finally we briefly discuss the importance of the results obtained herein to designing compounds with large damping capabilities. The answer, as discussed in a previous paper [8] depends on the application and what stresses levels are anticipated. If the design stresses are low, porous solids would be recommended. For high stress applications, and severe environments, where porous solids would not be suitable, either of the un-annealed solid solution compositions would yield the highest W_d values at the highest stresses.

6. Summary and conclusions

The ternaries, Ti_3AlC_2, Ti_2AlC and their solid solutions, Ti_3AlCN, $Ti_2Al(C_{0.5}N_{0.5})$ are KNE solids. Upon cyclic compression, fully, and spontaneously reversible hysteretic stress strain loops are generated. The microscale model developed to explain kinking nonlinear elasticity – in which ε_{NL} and W_d scale with σ^2 and W_d scales with ε_{NL} – is in excellent agreement with the experimental results. In sharp contrast to hexagonal metals, all the results shown here fall on straight lines implying 2α not a function of stress, even at stresses of the order of 650 MPa. The corresponding curves for coarse-grained Mg and Co polycrystalline samples, one the other hand, clearly deviate from linearity at higher stresses, suggesting that 2α is a function of stress.

This work also confirms [1,2,9,10] that the following factors, all embodied in Eq. (5), affect the size and shapes of the reversible loops:

(a) Grain size: the larger the grain size, the larger 2α and the lower the threshold stresses, which, for a given α, results in larger W_d values. The size to which the dislocation loops can grow is also larger.
(b) Matrix constraints or lack thereof: This factor, not well captured in our model, but related to the effective grain size, is an important consideration that explain why, at a given stress, porous solids can dissipate more energy than fully dense solids. It also presumably explains why the two solid solution samples, with bimodal distributions in their grain sizes were more resistant to kinking, and yielded higher Ω/b values, than their larger grained counterparts. Once the fine-grains were annealed out, the kinking occurred at significantly lower σ_t values, with concomitantly lower Ω/b values.
(c) Ω/b: For a given ε_{NL} strain, the higher the Ω/b values the higher W_d (Fig. 5c). The most important factor influencing Ω/b in this work appears to be grain size (Fig. 6). The relationship between 2α and Ω/b appears to follow Hall-Petch's.
(d) Because the ratio m_1/m_2 is proportional to Ω/b, it follows that the same micromechanism, viz. IKBs, responsible for the nonlinear strain is also responsible for W_d.

Acknowledgment

This work was supported by Army Research Office (DAAD19-03-1-0213).

References

[1] A.G. Zhou, M.W. Barsoum, S. Basu, S.R. Kalidindi, T. El-Raghy, Acta Mater. 54 (2006) 1631–1639.
[2] M.W. Barsoum, T. Zhen, A. Zhou, S. Basu, S.R. Kalidindi, Phys. Rev. B 71 (2005) 134101.
[3] M.W. Barsoum, A. Murugaiah, S.R. Kalidindi, T. Zhen, Y. Gogotsi, Carbon 42 (2004) 1435–1445.
[4] M.W. Barsoum, A. Murugaiah, S.R. Kalidindi, T. Zhen, Phys. Rev. Lett. 92 (2004) 255508.
[5] M.W. Barsoum, T. Zhen, S.R. Kalidindi, M. Radovic, A. Murugaiah, Nat. Mater. 2 (2003) 107–111.

[6] P. Finkel, A.G. Zhou, S. Basu, O. Yeheskel, M.W. Barsoum, Appl. Phys. Lett. 94 (2009) 241904.
[7] S. Amini, A. Zhou, S. Gupta, A. DeVillier, P. Finkel, M. Barsoum, J. Mater. Res. 23 (2008) 2157–2165.
[8] M. Fraczkiewicz, A.G. Zhou, M.W. Barsoum, Acta Mater. 54 (2006) 5261–5270.
[9] A.G. Zhou, S. Basu, M.W. Barsoum, Acta Mater. 56 (2008) 60–67.
[10] A. Zhou, M. Barsoum, Metal. Mater. Trans. A 40 (2009) 1741–1756.
[11] S. Basu, A.G. Zhou, M.W. Barsoum, J. Mater. Res. 23 (2008) 1334–1338.
[12] S. Basu, M.W. Barsoum, J. Mater. Res. 22 (2007) 2470–2477.
[13] S. Basu, A. Zhou, M.W. Barsoum, J. Struct. Geol. 31 (2009) 791–801.
[14] M.W. Barsoum, Prog. Solid State Chem. 28 (2000) 201–281.
[15] M.W. Barsoum, M. Ali, T. El-Raghy, Metal. Mater. Trans. A 31 (2000) 1857–1865.
[16] M.W. Barsoum, T. El-Raghy, J. Am. Ceram. Soc. 79 (1996) 1953–1956.
[17] T. Zhen, M.W. Barsoum, S.R. Kalidindi, Acta Mater. 53 (2005) 4163–4171.
[18] J.Y. Wang, Y.C. Zhou, J. Phys.: Condens. Matter 15 (2003) 5959–5968.
[19] Y.C. Zhou, J.X. Chen, J.Y. Wang, Acta Mater. 54 (2006) 1317–1322.
[20] I. Salama, T. El-Raghy, M.W. Barsoum, J. Alloys Compd. 347 (2002) 271–278.
[21] J.Y. Wang, Y.C. Zhou, J. Phys.: Condens. Matter 16 (2004) 2819–2827.
[22] N.A. Phatak, S.K. Saxena, Y. Fei, J. Hu, J. Alloys Compd. 475 (2009) 629–634.
[23] M. Radovic, A. Ganguly, M. Barsoum, J. Mater. Res. 23 (2008) 1517–1521.
[24] T. Scabarozi, A. Ganguly, J. Hettinger, S. Lofland, S. Amini, P. Finkel, T. El-Raghy, M. Barsoum, J. Appl. Phys. 104 (2008) 073713–173713.
[25] N. Orlovskaya, H. Anderson, M. Brodnikovskyy, M. Lugovy, M.J. Reece, J. Appl. Phys. 100 (2006) 026102.
[26] Y.L. Hao, S.J. Li, B.B. Sun, M.L. Sui, R. Yang, Phys. Rev. Lett. 98 (2007) 216405.
[27] Y.L. Hao, S.J. Li, S.Y. Sun, C.Y. Zheng, R. Yang, Acta Biomater. 3 (2007) 277–286.
[28] C.H. Caceres, T. Sumitomo, M. Veidt, Acta Mater. 51 (2003) 6211–6218.
[29] G.E. Mann, T. Sumitomo, C.H. Caceres, J.R. Griffiths, Mater. Sci. Eng. A 456 (2007) 138–146.
[30] O. Muránsky, D.G. Carr, P. Sittner, E.C. Oliver, Int. J. Plasticity 25 (2009) 1107–1127.
[31] R. Telle, A. Momozawa, D. Music, J.M. Schneider, J. Solid State Chem. 179 (2006) 2850–2857.
[32] J.M. Molina-Aldareguia, J. Emmerlich, J.-P. Palmquist, U. Jansson, L. Hultman, Scripta Mater. 49 (2003) 155–160.
[33] O. Wilhelmsson, P. Eklund, F. Giuliani, H. Hogberg, L. Hultman, U. Jansson, Appl. Phys. Lett. 91 (2007) 123124.
[34] O. Wilhelmsson, P. Eklund, H. Höberg, L. Hultman, U. Jansson, Acta Mater. 56 (2008) 2563–2569.
[35] W. Tian, Z. Sun, H. Hashimoto, Y. Du, J. Mater. Sci. 44 (2009) 102–107.
[36] G. Zhang, Z. Wei, R.E. Ferrell, Appl. Clay Sci. 46 (2009) 429–432.
[37] R.A. Lebensohn, M. Montagnat, P. Mansuy, P. Duval, J. Meysonnier, A. Philip, Acta Mater. 57 (2009) 1405–1415.
[38] F.C. Frank, A.N. Stroh, Proc. Phys. Soc. B 65 (1952) 811–821.
[39] D. Hull, Introduction to Dislocation, Pergamon Press, Oxford, 1965.
[40] R.E. Reed-Hill, E.P. Dahlberg, J.W.A. Slippy, Trans. AIME 233 (1965) 1766–1771.
[41] B. Manoun, S.K. Saxena, G. Hug, A. Ganguly, E.N. Hoffman, M.W. Barsoum, J. Appl. Phys. 101 (2007) 113523.
[42] Z.M. Sun, A. Murugaiah, T. Zhen, A. Zhou, M.W. Barsoum, Acta Mater. 53 (2005) 4359–4366.
[43] V. Nikolay, M. Barsoum, J. Am. Ceram. Soc. 83 (2000) 825–832.
[44] T. El-Raghy, M.W. Barsoum, J. Am. Ceram. Soc. 82 (1999) 2849–2854.
[45] S. Amini, M.W. Barsoum, Mater. Sci. Eng. A, in press (2010).
[46] M.W. Barsoum, T. El-Raghy, Metal. Mater. Trans. A 30 (1999) 363–369.